Quadrupole-mode transfer function and the nonlinear Mathieu instability

Weiming Guo* and S. Y. Lee

Indiana University, Bloomington, Indiana 47408

(Received 23 February 2002; published 19 June 2002)

We show that the quadrupole-mode transfer function (QTF) is a powerful nondestructive tool to measure properties of dynamical systems. In particular, we discuss the feasibility of using the QTF to measure the betatron tunes and the beam emittances with a beam-position monitor system. The QTF can also be used to compensate the optical mismatch during the beam injection process. However, it is less effective than the rf dipole method in overcoming the intrinsic spin resonances for polarized beam acceleration.

I. INTRODUCTION

The parametric resonances of dynamical systems have been studied extensively in the past. It is a powerful tool in characterizing chaos and properties of many dynamical systems [1]. Naturally, it has many applications in the physics of beams. For example, the parametric resonances in the longitudinal phase space induced by rf cavity voltage and phase modulations have been employed to manipulate beam bunch for various applications [2,3]. The rf cavity phase modulation induces dipole-mode oscillations of the beam bunch in the synchrotron phase space, and thus it may be used to actively compensate the synchro-betatron coupling resonances [4]. It can also be used to create a bounded chaotic region in the longitudinal phase space for a controlled bunch dilution [5]. The rf cavity voltage modulation at the second synchrotron sideband has also been applied to alleviate the coupled bunch instability driven by the parasitic modes [6], and to manipulate bunch shape for bunch length compression [7].

The idea of bunch manipulation has recently been extended to the transverse phase space, where the coherent dipole-mode excitation driven by a transverse rf dipole field has been successfully applied to overcome intrinsic spin resonances at the alternating-gradient synchrotron (AGS) [8]. The rf dipole, excited adiabatically, changes the beam closed orbit without changing the phase-space area. Since the coherent betatron oscillation amplitude vs the rf dipole modulation tune is well known, one can use this method to measure the betatron tune without suffering emittance dilution [8]. However, a coherent betatron dipole-mode oscillation can change the betatron tune that one is measuring. This will produce additional uncertainty in the determination of the betatron tune.

With advanced data analysis techniques, the dipole-mode transfer function can be used to reveal hidden dynamical variables in many complicated dynamical systems. Some of these data analysis techniques are the orbit response matrix method [9], and the model independent analysis method [10]. Both techniques have been successfully implemented in improving the performance of high intensity accelerators.

On the other hand, the power of quadrupole-mode transfer function has not been explored. There is only a limited study on beam dynamics for a time dependent transverse quadru-

pole field. A fast field-changing quadrupole can be used to produce betatron tune jump for overcoming intrinsic spin resonances [11,12], and for studying a strong betatron resonance [13]. Similarly, a harmonic tune modulation can be used to study the effect of enhanced-diffusion process at a betatron resonance [14]. This paper studies physics of a transverse quadrupole-mode transfer function and its applications, and the corresponding dynamical systems associated with the nonlinear Mathieu instability.

We organize this paper as follows. In Sec. II, the effective Hamiltonian in the presence of an rf quadrupole is reviewed, where the stable and unstable fixed points are discussed. Section III examines some applications of rf quadrupole-mode transfer function, such as measuring the beam emittance and the betatron tune by using an rf quadrupole and the quadrupole beam-transfer function of beam-position monitor (BPM), compensating the injection mismatch with rf quadrupoles, and overcoming the intrinsic spin resonances with coherent quadrupole excitation. The conclusion is given in Sec. VI. Properties of the nonlinear Mathieu instability and the strength of the quadrupole-mode transfer function for the Boltzmann beam distribution are discussed in the Appendixes.

II. BEAM DYNAMICS WITH rf QUADRUPOLES

In the Frenet-Serret coordinate system, the Hamiltonian for particle motion in the transverse phase-space coordinates, in the presence of rf quadrupoles, is [15]

$$H = \frac{1}{2}y'^2 + \frac{1}{2}K_y(s)y^2 + \frac{1}{2}K_{rf}(s)y^2 \cos(\omega_m t + \theta_0), \quad (1)$$

where y, y' are phase-space coordinates representing either the horizontal or vertical phase space, $K_y(s) = B_1(s)/(B\rho)$ is the designed quadrupole strength of the accelerator lattice, $B_1(s) = \partial B_z/\partial x$ is the gradient function of the vertical magnetic flux density, $K_{rf}(s) = B_{1,rf}(s)/(B\rho)$ is the strength of rf quadrupole, $B\rho$ is the magnetic rigidity of the beam, s is the longitudinal coordinate, ω_m is the modulation angular frequency, and θ_0 is the initial phase angle of the rf quadrupole. Transforming the phase-space coordinate to the action-angle variables, one obtains an effective Hamiltonian near betatron sideband as (see the Appendix A and Ref. [15])

$$H(J_y, \phi_y) \approx \nu_y J_y + J_y C_1 \cos(2\phi_y - n\theta - \nu_m\theta + \chi), \quad (2)$$

*Electronic address: weguo@indiana.edu

where we assume that the modulation tune $\nu_m = \omega_m/\omega_0$ is near a quadrupole betatron sideband $|2\nu_y - n|$ and ω_0 is the angular revolution frequency of the beam. The Hamiltonian tori will be resonantly deformed.

A. Linear Mathieu instability

We transform the Hamiltonian (2) into a *resonance rotating frame* by using the generating function $F_2 = (\phi_y - \frac{1}{2}n\theta - \frac{1}{2}\nu_m\theta + \chi)J$ to obtain a new Hamiltonian:

$$H(\psi, I) = \delta I + C_1 I \cos 2\psi, \tag{3}$$

where $I = J$, $\psi = \phi_y - \frac{1}{2}n\theta - \frac{1}{2}\nu_m\theta + \chi$, and $\delta = |\nu_y - \frac{1}{2}n| - \frac{1}{2}\nu_m$ is called the *resonance proximity parameter*. Since the Hamiltonian (3) is time (θ) independent, the Hamiltonian is a constant of motion. It is equivalent to take the Poincaré surface of section at every $1/\nu_m$ turns.

In the region of $-|C_1| \leq \delta \leq +|C_1|$, the beam encounters the linear Mathieu instability driven by the rf quadrupole. The Hamiltonian (3) is stable when $|\delta| > |C_1|$. Introducing the normalized coordinates: $X = \sqrt{2I} \cos\psi$ and $P = -\sqrt{2I} \sin\psi$, the Hamiltonian is transformed to

$$H = \frac{1}{2}(\delta + C_1)X^2 + \frac{1}{2}(\delta - C_1)P^2. \tag{4}$$

A torus associated with a constant Hamiltonian value is elliptical, and the fixed stable point is located at the origin with $I_{\text{sfp}} = 0$, or $X_{\text{sfp}} = P_{\text{sfp}} = 0$. The aspect ratio of the ellipse is $\sqrt{|(\delta + C_1)/(\delta - C_1)|}$. Adjusting the δ or C_1 parameters, one can adjust the shape of admittance ellipse, and thus the rf quadrupole can be used to compensate injection mismatch.

B. Nonlinear Mathieu instability

When a detuning term is included, e.g., in the presence of octupole magnets, the Hamiltonian becomes

$$H = \delta I + C_1 I \cos 2\psi + \frac{1}{2}\alpha_{yy} I^2, \tag{5}$$

where we neglect effects of higher order nonlinear resonances. The nonlinear detuning parameter α_{yy} may arise from the space charge force, the concatenating effects of sextupoles, and other higher order multipoles. For example, the detuning parameter due to an octupole is $\alpha_{yy} = (1/16\pi)\oint(B_3/B\rho)\beta_y^2 ds$, where $B_3 = \partial^3 B_z/\partial x^3$ is the octupole field strength.

Fixed points can be obtained from the Hamiltonian's equation: $\dot{I} = 0$ and $\dot{\psi} = 0$, where the overdot represents the time derivative. The general property of the Hamiltonian (5) is discussed in Appendix B. It depends only on two independent parameters: $\Delta = \delta/\alpha_{yy}$ and $c_1 = -C_1/\alpha_{yy}$. For example, if $\alpha_{yy} < 0$ and $C_1 > 0$, the stable fixed points are given by

$$I_{\text{sfp}} = \begin{cases} -\dfrac{1}{\alpha_{yy}}(\delta + C_1) & \text{if} \quad \delta > -C_1, \\ 0 & \text{if} \quad \delta > C_1 \quad \text{and} \quad \delta < -C_1, \end{cases} \tag{6}$$
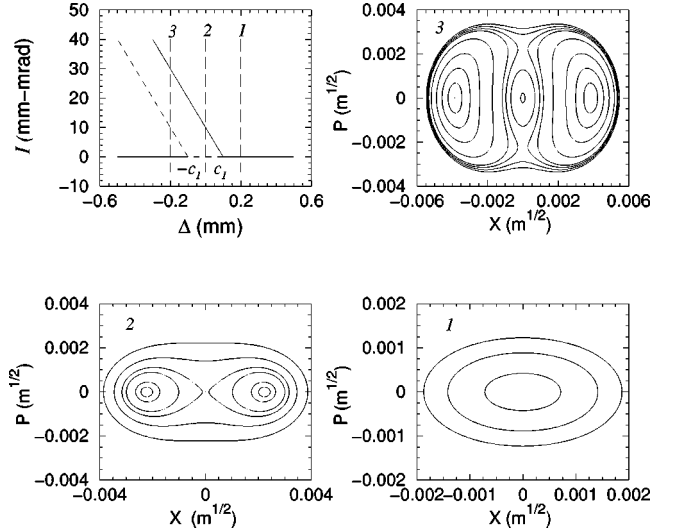
FIG. 1. Top left: stable (solid line) and unstable (short dashed line) fixed points vs the effective resonance proximity parameter $\Delta = \delta/\alpha_{yy}$ for the effective resonance strength parameter $c_1 = 0.10$ mm. The plots labeled (1), (2), and (3) correspond to the vertical long-dashed lines marked as 1, 2, and 3, respectively. The Hamiltonian is $H = \Delta I - c_1 I \cos 2\psi + \frac{1}{2}I^2$ with $X = \sqrt{2I}\cos\psi$ and $P = -\sqrt{2I}\sin\psi$.

with $\psi_{\text{sfp}} = 0$ and π. The corresponding unstable fixed points are located at

$$I_{\text{ufp}} = \begin{cases} -\dfrac{1}{\alpha_{yy}}(\delta - C_1) & \text{if} \quad \delta > C_1, \\ 0 & \text{if} \quad -C_1 < \delta < C_1, \end{cases} \tag{7}$$

with $\psi_{\text{ufp}} = \pi/2$ and $3\pi/2$. The top-left plot of Fig. 1 shows the action of the fixed points vs the parameter Δ for a parameter $c_1 = 0.10$ mm (see Appendix B). The plots labeled (1), (2), and (3) correspond to the parameters marked with the vertical long-dashed lines 1, 2, and 3 respectively. Note that the region (1) is below the bifurcation threshold and the phase space is bifurcated into two islands in region (2) and three islands in region (3).

III. APPLICATIONS OF RF QUADRUPOLE-MODE TRANSFER FUNCTION

A. Emittance and tune measurement

It was first pointed out by Miller that the signal from a BPM can be used to derive the beam moments [16], and thus the beam emittance can be determined [17]. There were considerable efforts to measure emittance using BPMs in linacs [18]. Application of this idea to storage ring has not been fully successful because the rms signal derived from a BPM is weak and the rms beamwidth cannot easily be modified by a quadrupole [19]. Here we present an idea in enhancing the weak rms signal for the measurement of emittance by the rf quadrupole-mode transfer function, and we carry out numerical simulation to justify our claims.

The induced surface charge density on a conducting cylinder by an infinitely long line charge is

$$\sigma(r,\phi,a,\Theta) = \frac{\lambda}{2\pi a} \frac{a^2 - r^2}{a^2 + r^2 - 2ar\cos(\Theta - \phi)}$$

$$= \frac{\lambda}{2\pi a}\left[1 + 2\sum_{i=1}^{\infty}\left(\frac{r}{a}\right)^k \cos k(\Theta - \phi)\right], \quad (8)$$

where $\lambda = N_{\mathrm{B}}e/(\sqrt{2\pi}\sigma_s)$ is the line-charge density, e is the charge of the orbiting particle, N_{B} is the number of particles in a bunch, σ_s is the rms bunch length, (r,ϕ) is the location of the line charge in cylindrical coordinate system, (a,Θ) is the position on the conducting cylinder with radius a. We expand the induced surface charge density in power series of r/a because the radius r of the charge particle is much smaller than the BPM chamber radius a. Let the beam distribution function be $\rho(x,x',z,z')$, where (x,x') and (z,z') are the transverse phase-space coordinates of betatron motion. The distribution function is normalized by $\int\rho(x,x',z,z')dxdx'dzdz' = 1$. The induced surface density on the cylinder becomes

$$\sigma(a,\Theta) = \int \sigma(x,z,a,\Theta)\rho(x,x',z,z')dxdzdx'dz'$$

$$= \frac{\lambda}{2\pi a}\left\{1 + 2\frac{\langle x\rangle}{a}\cos\Theta + 2\frac{\langle z\rangle}{a}\sin\Theta \right.$$

$$\left. + 2\left(\frac{\langle x^2\rangle - \langle z^2\rangle}{a^2}\right)\cos 2\Theta + 4\frac{\langle xz\rangle}{a^2}\sin 2\Theta + \cdots\right\}.$$

$$(9)$$

When an rf quadrupole is adiabatically turned on, where the modulation tune is near a betatron quadrupole-mode sideband, the bunch distribution will follow the invariant ellipse shown in Eq. (4), and the ellipse rotates at a tune of $\nu_{\mathrm{m}}/2$. The rms beamwidth becomes

$$\langle x^2\rangle = \langle x\rangle^2 + \frac{1}{2}(\langle X^2\rangle + \langle P_x^2\rangle) + \frac{1}{2}(\langle X^2\rangle - \langle P_x^2\rangle)\sin\nu_m\theta,$$

$$(10)$$

where $X = \sqrt{2\beta_x I_x}\cos\psi_x$ and $P_x = -\sqrt{2\beta_x I_x}\sin\psi_x$ are the normalized betatron phase-space coordinates. A quadrupole pickup will see a dominant harmonic of ν_{m}, i.e.,

$$q_2 = \frac{\sigma(a,0) + \sigma(a,\pi) - \sigma\left(a,\frac{\pi}{2}\right) - \sigma\left(a,\frac{3\pi}{2}\right)}{\sigma(a,0) + \sigma(a,\pi) + \sigma\left(a,\frac{\pi}{2}\right) + \sigma\left(a,\frac{3\pi}{2}\right)}$$

$$= \frac{1}{a^2}(b_0 + b_1\cos\nu_m\theta), \quad (11)$$

where

$$b_0 = 2(\langle x\rangle^2 - \langle z\rangle^2 - \langle z^2\rangle) + \langle X^2\rangle + \langle P_x^2\rangle, \quad (12)$$

$$b_1 = \langle X^2\rangle - \langle P_x^2\rangle, \quad (13)$$
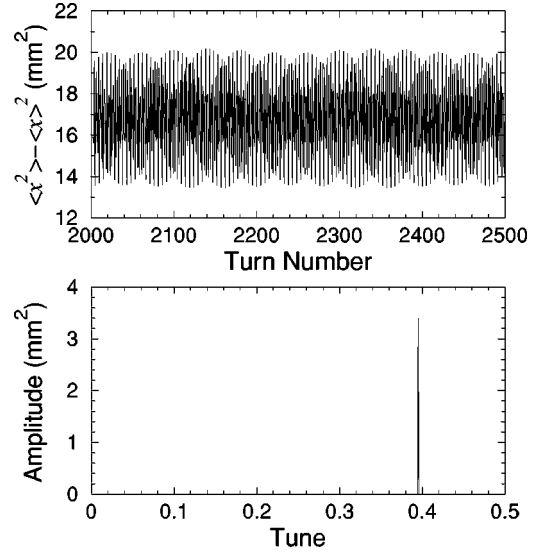
FIG. 2. Top: the second moment ($\langle x^2\rangle - \langle x\rangle^2$) derived from numerical simulation with parameters $\delta = 0.0025$, $C_1 = 0.0005$, $\nu_y = 8.7$, and $\nu_{\mathrm{m}} = 0.395$. Bottom: fast Fourier transform (FFT) spectrum of the second moment, where we obtain $b_0 = 3.405 \times 10^{-5}$ m^2 and $b_1 = 6.7\times 10^{-6}$ m^2. Note that b_0 and b_1 are defined as twice the Fourier amplitude.

and $\sqrt{\langle z^2\rangle}$ is the rms beamwidth in z direction. Although the dc component b_0 of the quadrupole moments q_2 is much larger than the modulation term b_1, the coefficient b_1 can, however, be accurately determined by a Fourier transformation of the quadrupole pickup. Here the coefficient b_1 is called the quadrupole-mode transfer function.

First, we consider a linear system without nonlinear betatron detuning. The stability condition for the linear Mathieu equation is $|\delta| > |C_1|$. The quadrupole-mode transfer function b_1 becomes (see Appendix C)

$$b_1 = \frac{2C_1\beta_x\epsilon_0}{\sqrt{\delta^2 - C_1^2}}, \quad (14)$$

where β_x is the betatron amplitude function at the location of the quadrupole-mode monitor.

Measurement of the b_1 coefficient vs the machine parameter $\delta = |\nu_x - \frac{1}{2}n| - \frac{1}{2}\nu_{\mathrm{m}}$ (by varying ν_{m}) can be used to determine the emittance ϵ_0. This provides a powerful experimental method to measure the beam emittance. Figure 2 shows the rms quadrupole moment as a function of revolution turns from an example of multiparticle simulation, where a sample of 10 000 particles is initially distributed in Gaussian distribution and the evolution of the distribution is governed by a one-turn linear map, an rf quadrupole kick, and a thin lens octupole kick. The strength of the rf quadrupole increases adiabatically in the first 1000 turns, while the modulation tune is maintained at a constant value, and the quadrupole moment, $\langle x^2\rangle - \langle x\rangle^2$, is measured from 2001 to 4000 turns. The coefficient b_1 is obtained by a Fourier analysis of the quadrupole moment data.

Figure 3 shows the parameter δ^2 vs the derived Fourier amplitude $1/b_1^2$ from data of multiparticle simulations with
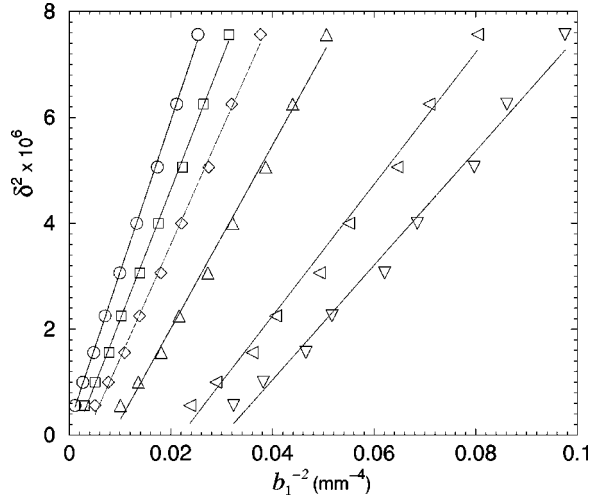
FIG. 3. Data obtained from a Fourier analysis of numerical simulations. The parameter δ^2 is plotted as a function of $1/b_1^2$. The parameters are $C_1 = 0.0005$ with $\alpha_{yy} = 0$, -100, -200, -400, -800, and -1000 m^{-1}, respectively, in different symbols from the leftmost to the rightmost. The straight line is shown to guide the eyes. The data are fitted to obtain the beam emittance. The input rms beam emittance of all simulations is 1π mm mrad, and the betatron amplitude function is 16.7 m.

an initial emittance 1.0π mm mrad and $C_1 = 0.0005$. Using Eq. (14), one can deduce emittance from the graph of δ^2 vs $1/b_1^2$ to be 0.97π mm mrad. We note that, indeed, the curve is linear for the linear betatron system, and the slope can be used to derive the emittance quite accurately. The intercept of the line with the vertical axis at $\delta = C_1$ can be used to determine the betatron tune.

In a realistic machine experiment, the accuracy of b_1 can be increased by increasing the number of measurement turns. Naturally, the number of data point is also limited by the machine stability, such as the tune stability, effects of beta-beat, etc., and the available memory of the data recording hardware.

Equation (14) is valid only for a linear betatron motion. However, Fig. 3 shows that δ^2 vs $1/b_1^2$ derived from numerical simulations for nonzero detuning parameter follows a family of nearly linear curves. The slope is reduced even for the same initial emittance. Appendix C discusses the effect of nonlinear detuning parameter on the beam distribution, and derives the b_1 coefficient for the Boltzmann beam distribution. We show that the slope is indeed reduced due to the nonlinear detuning parameter. Nevertheless, we can also derive the beam emittance and the tune of the dynamical system by using a phenomenological ansatz:

$$b_1 = \frac{2C_1\beta_x\epsilon_0}{\sqrt{(\delta + F\alpha_{xx}\epsilon_0)^2 - C_1^2}}, \quad (15)$$

where the nonlinear detuning coefficient α_{xx} can be accurately measured by using the method proposed in Ref. [20]. The derived emittance agrees well with the input emittance as shown in Fig. 4 with $F \approx 2.5 \pm 0.2$ for both Gaussian and
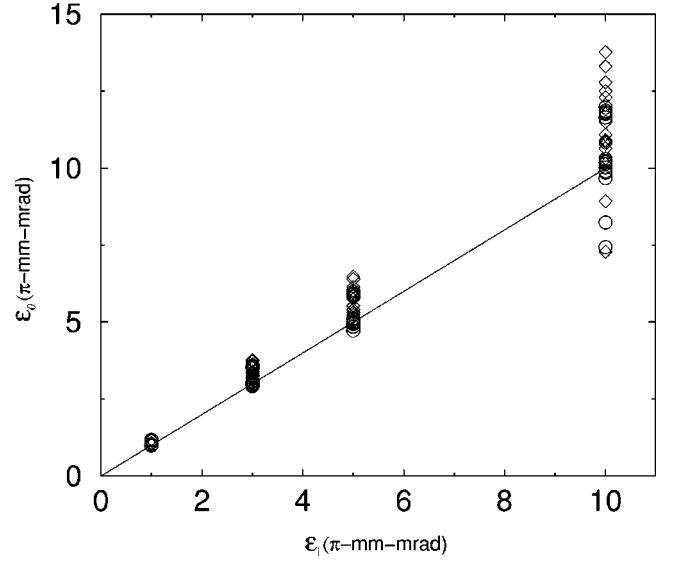
FIG. 4. Comparison between the measured emittance (ϵ_o from numerical simulation data) and the initial input emittance (ϵ_i horizontal axis). A total of 150 sets of numerical simulation data with different machine parameters (C_1 ranging from 0.0005 to 0.005, and α_{xx} ranging from 0 to -1000 m^{-1}) and different initial beam distribution functions [Gaussian (circles) and uniform (diamonds)] are included in this plot for comparison. The spread arises essentially from the nonlinear detuning, and the strength of the C_1 parameter.

uniform distributions. Exact expression for the b_1 coefficient for a Boltzmann distribution is derived in Appendix C.

For an actual beam-emittance measurement, the machine operation condition should be set such that it stays away from the nonlinear Mathieu bifurcation region, i.e., in the region (1) of Fig. 1. The procedure to measure beam emittance in a storage ring goes as follows: (1) Minimize the linear coupling, and measure the nonlinear detuning parameter α_{xx}; (2) Determine the rf quadrupole strength C_1, using the method derived in Appendix A; (3) Measure the quadrupole transfer function b_1 as a function of the modulation tune ν_m (or the resonance proximity parameter δ); (4) Use the measured data of b_1 vs δ to determine the emittance. The parameter C_1 depends on the strength of the rf quadrupole field and the value of the betatron amplitude function. It should not be too large to cause large betatron-function perturbation.

B. Mismatch correction

Optical mismatch during the injection can cause unwanted emittance dilution. Let the acceptance ellipse at the injection point of a synchrotron be

$$\gamma y^2 + 2\alpha yy' + \beta y'^2 = \epsilon_0, \quad (16)$$

where α, β, γ are the Courant-Snyder parameters of a synchrotron. The injection ellipse is

$$\gamma_1 y^2 + 2\alpha_1 yy' + \beta_1 y'^2 = \epsilon_0 \quad (17)$$

for a mismatched injection optics, where $\alpha_1, \beta_1, \gamma_1$ are the Courant-Snyder parameters from the injection line. Trans-

forming the injection ellipse into the normalized phase space of the ring optics with $Y=(1/\sqrt{\beta})y$ and $P=(1/\sqrt{\beta})(\beta y' + \alpha y)$, we find

$$a_1 Y^2 + a_2 Y P + a_3 P^2 = \epsilon_0, \qquad (18)$$

where $a_1 = \beta/\beta_1 + (\alpha_1\beta - \beta_1\alpha)^2/\beta\beta_1$, $a_2 = 2\alpha_1\beta - \alpha\beta_1/\beta$, and $a_3 = \beta_1/\beta$. The major and minor axes of the ellipse are given by $F_+ = (F_{mm} + \sqrt{F_{mm}^2 - 1})^{1/2}$ and $F_- = (F_{mm} - \sqrt{F_{mm}^2 - 1})^{1/2}$, where the mismatch factor F_{mm} is

$$F_{mm} = \frac{1}{2}(\gamma_1\beta + \beta_1\gamma - 2\alpha_1\alpha). \qquad (19)$$

The mismatch angle between the major axis and Y axis is

$$\psi_{mm} = \frac{1}{2}\arctan\left(\frac{a_2}{a_3 - a_1}\right). \qquad (20)$$

The ellipse of the mismatched injection beam will rotate because of the betatron motion. If the betatron motion were linear, the injection ellipse would rotate forever without emittance dilution. In the presence of nonlinear detuning, the bunch will filament and fill an area of πF_+^2. The rms emittance of this diluted beam depends on the particle distribution, and the rms emittance dilution factor is approximately F_{mm}.

1. Mismatch compensation for linear systems

Since the invariant torus is naturally elliptical when the rf quadrupole is modulating at $\nu_m \approx |2\nu_y - n|$, the torus can be used to compensate the mismatch. In other words, the admittance ellipse can be adjusted by an rf quadrupole such that it matches the injected beam. Note that if the injected beam is off-center, additional dipole is needed to compensate the closed orbit, i.e., the rf quadrupole can only modify the Courant-Snyder parameters.

To match the ellipses, we need to adjust the shape and orientation of the acceptance ellipse. When the rf quadrupole is located at the injection point, the match conditions are

$$\frac{C_1}{\delta} = \frac{F_+^2 - F_-^2}{F_+^2 + F_-^2} \qquad (21)$$

and

$$\theta_0 = \begin{cases} (\pi - 2\psi_{mm})/\nu_m & \text{for} \quad \delta > 0, \\ \theta_0 = 2\psi_{mm}/\nu_m & \text{for} \quad \delta < 0, \end{cases} \qquad (22)$$

where ψ_{mm}, F_+, and F_- are mismatch phase and factors, and θ_0 is the rf quadrupole initial phase angle. If the rf quadrupole is not located at the injection point, the phase difference between the rf quadrupole and the injection point should be added to or subtracted from ψ_{mm}. After the beam injection, we can adiabatically turn off the rf quadrupole.

Figure 5 shows the evolution of an injection ellipse in a numerical simulation where the betatron functions for the acceptance ellipse are $\alpha = 1.5$, $\beta = 16.692$ m, and $\gamma = 0.1947$ m^{-1}, and the betatron amplitude functions of the injection ellipse are $\alpha_1 = 1.4$, $\beta_1 = 12.6$ m, and γ_1
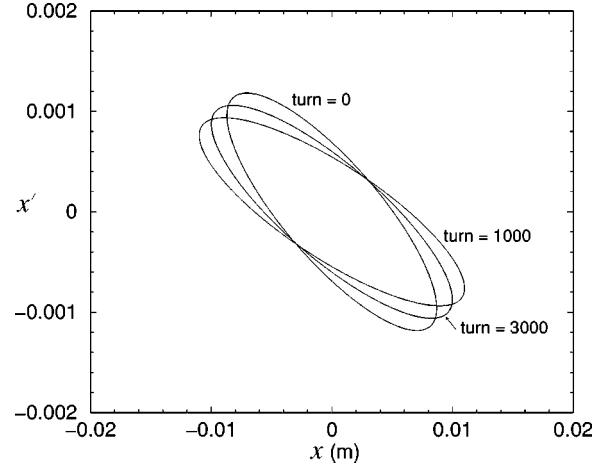
FIG. 5. The mismatched beam ellipse with $I = I_0$ at the injection (0th turn) is captured by an rf quadrupole, and the rf quadrupole strength is adiabatically turned off to restore the matched beam condition at the 3000th turn. The beam ellipse at the 1000th turn is also shown for reference.

$= 0.235$ m^{-1}. The corresponding mismatch factors are $F_{mm} = 1.08728$, $F_+ = 1.2305$, and $F_- = 0.81268$. The mismatched ellipse at the first-turn is snapped by the ellipse induced by an additional rf quadrupole, where the parameters for the rf quadrupole are $\delta = 0.01$, $C_1 = 0.0038087$, and $\theta_0 = 1.05649$. The rf quadrupole is adiabatically turned off from 2000 to 3000 turns. The ellipses at injection (0th turn), at 1000th turn, and 3000th turn are shown in Fig. 5. The beam ellipses can be perfectly matched by an rf quadrupole.

2. Mismatch compensation employing nonlinear Mathieu instability island

In many accelerators, the nonlinear betatron detuning terms are unavoidable. The method discussed in the preceding section can still be applied in the parametric region (1) of Fig. 1. However, we can also use the nonlinear Mathieu instability island in region (3) of Fig. 1 for mismatch compensation. Appendix B discusses the general properties of the nonlinear Mathieu Hamiltonian. Figure 6 shows an example of the phase-space ellipse for a nonlinear Mathieu Hamiltonian (5) with parameters $\delta = 0.02$, $C_1 = 0.007464$, and $\alpha_{yy} = -100$ m^{-1}. The Hamiltonian values of these tori are
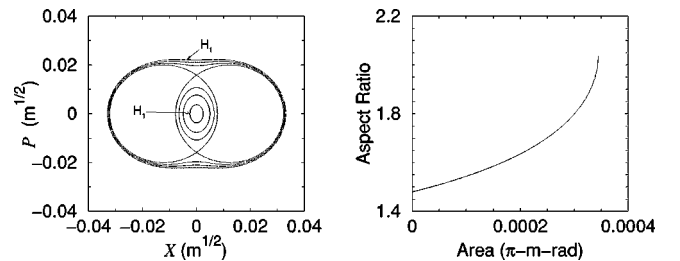
FIG. 6. Left: the invariant tori of the nonlinear Mathieu Hamiltonian with parameters: $\delta = 0.02, C_1 = 0.007464$, $\alpha_{yy} = -100$ m^{-1}. Right: the ratio $\sqrt{I_{max}/I_{min}}$ as a function of the phase-space area of invariant tori inside the middle island.

$H_1 = 8.27 \times 10^{-8}$ m and $H_{\text{sfp}} = 7.86 \times 10^{-7}$ m. The invariant torus rotates in the phase space at a tune of $\nu_m/2$.

To achieve mismatch compensation, the phase-space area of an ellipse enclosed by the separatrix torus must be larger than the phase-space area of the injected beam, and the aspect ratio must be equal. The action I of a given torus at a constant H is

$$I = \frac{1}{\alpha_{yy}} [-(\delta + C_1 \cos 2\psi) + \sqrt{(\delta + C_1 \cos 2\psi)^2 + 2\alpha_{yy} H}]$$

(23)

for the inner island (see the left plot of Fig. 6). The aspect ratio of a torus is

$$\frac{I_{\psi=\pi/2}}{I_{\psi=0}} = \frac{-(\delta - C_1) + \sqrt{(\delta - C_1)^2 + 2\alpha_{yy} H}}{-(\delta + C_1) + \sqrt{(\delta + C_1)^2 + 2\alpha_{yy} H}},$$

(24)

and the phase-space area is $(1/2\pi) \oint I d\psi$. The right plot of Fig. 6 shows the aspect ratio as a function of the available phase area in π m rad. The formula for the bucket size is complicated. However, one can use the condition that the minimum action $I_{\text{sx,min}}$ of the separatrix torus must be larger than $6\epsilon_0$ of the injected beam to ensure enough phase-space area for the injected beam, i.e.,

$$I_{\text{sx, min}} = -\frac{\delta}{\alpha_{yy}} \left(1 - \sqrt{\frac{C_1}{\delta}}\right)^2 > 6\epsilon_0.$$

(25)

In summary, the procedure of mismatch compensation is given as follows. First, we adjust C_1/δ to shape the aspect ratio of an admittance torus, change δ/α_{yy} to provide enough bucket area for the injection beam, and adjust the the phase of the rf quadrupole to match the orientation of the ellipse with match conditions: $\sqrt{I_{\max}/I_{\min}} = F_+/F_-$, and $\theta_0 = (\pi - 2\psi_{\text{mm}})/\nu_m$, where ψ_{mm}, F_+, and F_- are mismatch phase and factors. Here the π in the θ_0 matching condition arises from the fact that the major axis of the ellipse is in the $\psi = \pi/2$ direction.

We should note that the shape of the tori is not exactly elliptical and the aspect ratio depends on the phase-space area (see Fig. 6), and hence it is difficult to compensate mismatch fully. In realistic applications, the ratio between the major and minor axes of a weakly mismatched injection ellipse in normalized phase-space is close to 1, hence we can choose $|\delta| \gg |C_1|$, where the aspect ratio is close to a constant if the beam emittance is small. We can also choose the aspect ratio matching condition only for the rms action $I_{\text{rms}} = \epsilon_0/2$ ellipse, where ϵ_0 is the rms beam emittance. Our simulations show that the final emittance can be well preserved by this simplified matching condition.

In our multiparticle simulations, we use identical mismatch parameters as we have used in the preceding section, i.e., the admittance ellipse parameters are $\alpha = 1.5$, $\beta = 16.692$ m, $\gamma = 0.1947$ m^{-1}, and the injection ellipse is defined by $\alpha_1 = 1.4$, $\beta_1 = 12.6$ m, and $\gamma_1 = 0.235$ m^{-1}. The mismatch factors are $F_{\text{mm}} = 1.087\,28$, $F_+ = 1.2305$, and $F_- = 0.812\,68$. Multiparticle simulations are carried out with 10 000 particles in Gaussian distribution at an initial rms emittance of 6.0π mm mrad. All particles are tracked for
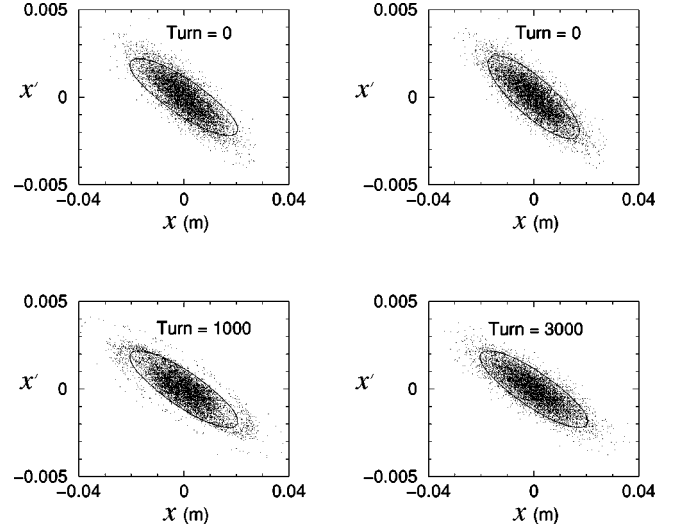
FIG. 7. Left plots: the injected beam is mismatched at the top-left plot. Filamentation is clearly shown in the bottom-left plot at the 1000th turn for the mismatched beam. Right plots: using nonlinear Mathieu resonance to match the injected beam shown in the top-right plot, we find that the beam emittance is preserved at the 3000th turn even in the presence of nonlinear detuning parameter. The solid lines in this graph show the 2σ admittance ellipse. See the text for parameters used in these simulations.

3000 turns, and the rf quadrupole is adiabatically turned off from 2001 to 3000 turns. Based on our discussion above, the parameters for the rf quadrupole and the octupole are set at $\delta = 0.02$, $\alpha_{yy} = -100$ m^{-1}, and $C_1 = 0.007\,464$ with a mismatch angle $\theta_0 = 1.0594$. The octupole was treated as a localized kick element. The left-top plot in Fig. 7 shows the initial mismatched beam injected into an accelerator, where the 2σ phase-space admittance ellipse is also shown. The left-bottom plot of Fig. 7 shows particle distribution in the phase space at 1000th turn, where one observes filamentation of particle distribution. On the other hand, if the rf quadrupole is properly implemented, the matched ellipse as shown in the top-right plot of Fig. 7, the resulting emittance is preserved as shown in the bottom-right plot of Fig. 7. The rms emittance measured at 3000th turn is about 6.48π mm mrad without mismatch compensation vs 6.01π mm mrad with mismatch compensation.

A slight increase of emittance arises from mismatch compensation using nonlinear Mathieu islands arises from torus deformation. The left plot of Fig. 8 shows the $\sqrt{10}\sigma$ ellipse at injection and the filamented ellipse at 3000th turn. On the other hand, if the ellipse is mismatched in the phase coordinate, the resulting phase-space dilution will be large as shown in the right plot of Fig. 8 for the 1σ ellipse, where the initial phase mismatch is $90°$. Results of numerical simulations also show that the emittance is not very sensitive to the aspect ratio, but more sensitive to the phase matching condition. Since the island tune of the Mathieu resonance island is highly nonlinear, the resulting emittance increase is limited. Clearly the mismatch compensation with nonlinear Mathieu island is not as good as that using the linear Mathieu phase-space distortion. The existence of octupole component can
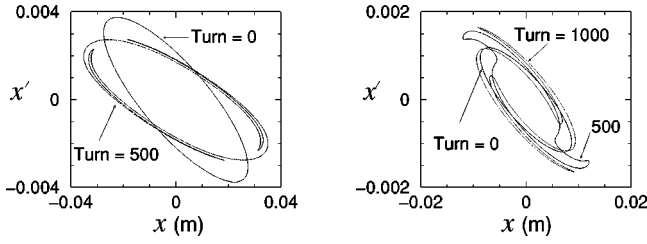
FIG. 8. For nonlinear Mathieu resonance islands, the invariant tori are not perfectly elliptical. However, the emittance growth is limited by the nonlinearity of these tori. The left plot shows that the $\sqrt{10}\sigma$ ellipse will evolve with filamentation. On the other hand, if the phase of the injection ellipse is mismatched by $90°$, the emittance dilution is much more severe. The right plot shows the evolution of the 1σ ellipse with an initial phase intentionally set at $\psi = \psi_0 + \pi/2$. We observe a much larger beam filamentation. Because the Mathieu island is highly nonlinear, the ellipse is tightly wrapped.

change the aspect ratio and limit the bucket size. Figure 9 shows the aspect ratio as a function of C_1 for different nonlinear detuning parameter α_{yy}.

C. Overcoming spin resonances

The particle spin precesses in synchrotron at a spin tune of $G\gamma$ per revolution, where $G=(g-2)/2$ is the Pauli anomalous g factor and γ is the Lorentz relativistic factor. During the polarized beam acceleration, the spin tune may sweep through many spin depolarizing resonances caused by the nonideal beam closed orbit and the betatron motion. There are a few innovative schemes invented to overcome these spin depolarization resonances [12]. For example, the rf dipole has been successfully used to generate a coherent dipole motion and induce spin flip to most particles in the beam and thus preserve the polarization of the beam for polarized beam acceleration through an intrinsic spin resonance [8]. However, the coherent dipole excitation produces two nearly overlapping spin resonances, i.e., the intrinsic spin resonance, and the induced spin resonance. Since an rf quadrupole can also induce coherent quadrupole-mode oscilla-
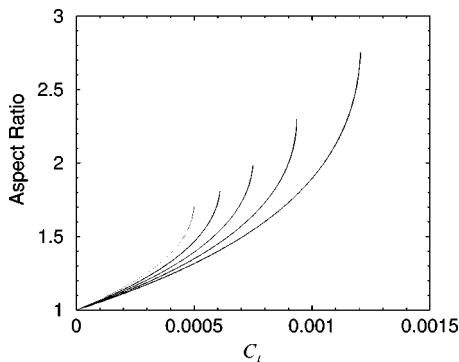
FIG. 9. The aspect ratio changes as a function of C_1 at the point $I_{\psi=0}=5.0\times10^{-7}$. $\delta=0.002$, from the inner to the outer $\alpha_{yy} = -1000, -800, -600, -400, -200$ in sequence. The curve ends when the edge of the bucket is reached.
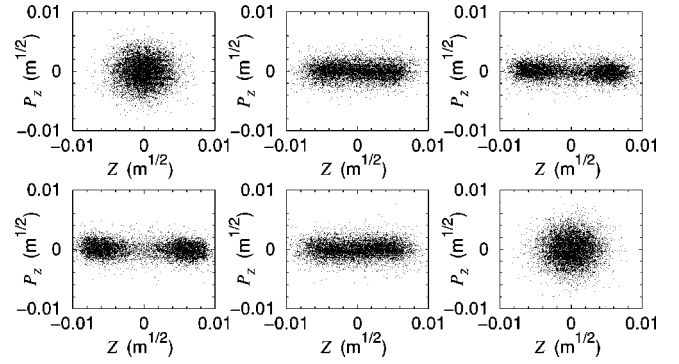
FIG. 10. The evolution of bunch distribution as the rf quadrupole parameters are adiabatically changed. The beam splits into two beamlets, and restore back to one. The normalized phase space in this plot is defined as $Z=\sqrt{2I}\cos\psi$ and $P_Z=-\sqrt{2I}\sin\psi$. Parameters used in the numerical simulations at the bottom-left plot are $\delta=-0.006256$, $C_1=0.01$, and $\alpha_{yy}=-200$ m^{-1}. The times corresponding to these Poincaré surfaces of section are marked in Fig. 11.

tion, it would be interesting to examine the capability of the rf quadrupole on the spin-resonance compensation.

To overcome spin resonance, we work with nonlinear Mathieu instability shown in Fig. 1. The beam manipulation procedure goes as follows. The rf quadrupole is initially adiabatically turned on to a preset value in a single fixed point region with $|\delta|>|C_1|$, then the modulation tune ν_m is adiabatically changed to the condition $|\delta|\leqslant|C_1|$, where the stable fixed point is bifurcated into two stable fixed points. In this region, the unstable fixed point is located at $I_{\mathrm{ufp}}=0$. Because all particles execute coherent betatron quadrupole-mode oscillations, the beam polarization can be maintained after passing through the spin resonance.

If the parameters of the rf quadrupole are changed adiabatically, particles will follow the Hamiltonian tori. Following the procedure stated in the preceding paragraph, particles will move into nonlinear Mathieu islands as shown in Fig. 10, where the times for the Poincaré surface of section (snapshot in the phase-space) are marked as diamond symbols in Fig. 11 with the corresponding machine parameters used in the multiparticle simulation. The snapshots of the Poincaré surfaces of the section are taken in the time sequence from the top-left plot in the first row to the bottom-right plot of the second row. It seems that there is little emittance increase if the procedure is carried out properly.

However, if we inspect the physics more closely, the procedure is intrinsically nonadiabatic, and emittance increase is unavoidable. Figure 12 shows the evolution of the 1σ ellipse of the corresponding multiparticle simulation shown in Fig. 10 at the exact time as shown in Fig. 11. As the phase-space is divided into two islands, the phase space ellipse is wound into two islands. When the procedure is reversed, these two disjoint ellipses can not be restored into the original one, and the emittance cannot be preserved during this process.

In most applications, the increase of beam emittance is, however, reasonably small. The left plot of Fig. 13 shows the rms emittance increment ratio for $\alpha_{yy}=-400$ m^{-1} ($\triangle$), -600 m^{-1} ($\diamond$), and -1000 m^{-1} ($\bigcirc$) as a function of
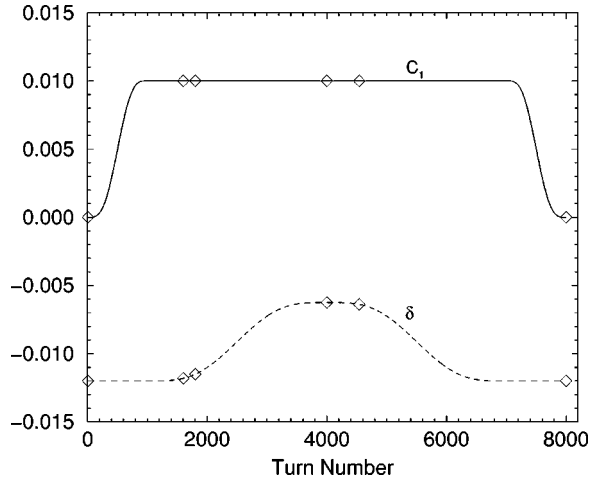
FIG. 11. The dashed and solid lines are the resonance proximity δ parameter and the rf quadrupole strength C_1 as functions of time (in revolution turns). The Poincaré surfaces of section plotted in Figs. 10 and 12 are marked as diamond symbols. The corresponding turn numbers are 0, 1600, 1800, 4000, 4540, and 8000.

the I_{sfp} by changing the δ parameter at a constant C_1 $= 0.0004$. Note that the emittance growth does not depend much on the α_{yy} parameter, but is a sensitive function of I_{sfp}. The emittance growth would be much larger if the I_{sfp} goes beyond the second bifurcation region. The right plot of Fig. 13 shows the emittance growth factor as a function of I_{sfp} for a given α_{yy} with different C_1 parameter. For a smaller C_1 parameter, one has to set the δ parameter near the bifurcation of three-island region to get the desired action I_{sfp}. The resulting emittance dilution becomes very large, because some particles are squeezed out of a bucket into another bucket. The adiabaticity condition is not fulfilled, and the emittance dilution is inevitable.

If we assume that the beam distribution around two stable fixed points of the Mathieu instability region is Gaussian, the spin flipping rate is given by the ensemble average of beam distribution with the Froissart-Stora formula, i.e.,

$$\frac{P_f}{P_i} = \frac{2}{1 + \pi\varepsilon_0^2/\alpha} \exp\left\{ -\frac{I_{\text{sfp}}}{\epsilon_0} \frac{\pi\varepsilon_0^2/\alpha}{1 + \pi\varepsilon_0^2/\alpha} \right\} - 1, \quad (26)$$
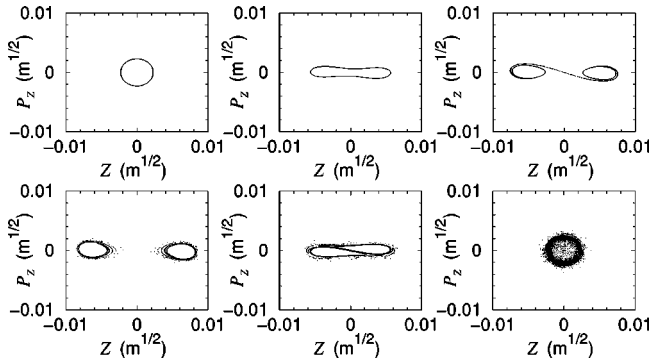
FIG. 12. The evolution of the 1σ ellipse in the beam manipulation where the beam is moved adiabatically through the Mathieu bifurcation point and back. Parameters used in this simulation at the bottom-left plot are $\delta = -0.006\,256$, $C_1 = 0.01$, and α_{yy} $= -200$ m^{-1}.
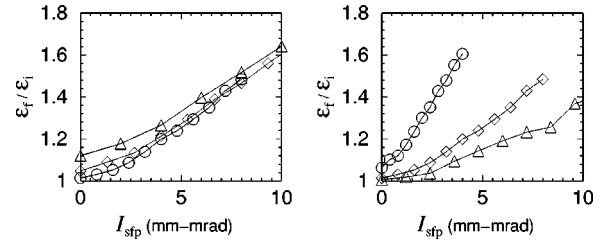
FIG. 13. Left: emittance increment ratio ϵ_f/ϵ_i after moving the beam to I_{sfp} and back for different α_{yy}. Parameters used in this calculation are $C_1 = 0.004$ with $\alpha_{yy} = -400$ m^{-1}($\triangle$), -600 m^{-1} ($\diamond$), and -1000 m^{-1} ($\bigcirc$), respectively. Right: emittance increment ratio after moving the beam to I_{sfp} and back for different parameter C_1. Here, we use $\alpha_{yy} = -1000$ m^{-1}, with C_1 $= 0.006$ ($\triangle$), 0.004 ($\diamond$), and 0.002 ($\bigcirc$), respectively.

where I_{sfp} is action at stable fixed point, ε_0 is the spin resonance strength for a particle with rms action $\frac{1}{2}\epsilon_0$, and α $= d(G\gamma)/d\theta$ is the acceleration rate.

Using the AGS parameter as our working example, the spin flipping rate is shown in Table I, where we use the parameters: $\alpha_{yy} = -200$ m^{-1}, $C_1 = 0.01$, $\delta = -0.006\,26$, and $\epsilon_0 = 1.66\pi$ mm mrad for the AGS beam to obtain I_{sfp} $= 18.7$ mm mrad. The polarized beam acceleration rate is $\alpha = 4.86 \times 10^{-5}$. On the other hand, we can calculate the polarization by carrying out ensemble average from the beam distribution. These two results are compared in the third and the fourth column of Table I. Note that the polarization based on Gaussian distribution slightly overestimate the final polarization value.

IV. CONCLUSION

In conclusion, we have studied the quadrupole-mode beam-transfer function and the dynamics of the nonlinear Mathieu instability. We show that the quadrupole-mode beam-transfer function can be used to measure the betatron tunes, beam emittances, to compensate beam mismatch during the injection, and to overcome intrinsic spin resonances for the polarized beam acceleration.

In the betatron tune measurement, the quadrupole beam-transfer function has the advantage of not changing the beam closed orbit, and thus the resulting measurement is less affected by the effect of feed downs from the higher order multipoles. We show clearly that the quadrupole-mode beam-transfer function is a powerful method to measure the beam emittance nondestructively, and to compensate the injection mismatch effectively. We, however, find that the quadrupole-mode beam-transfer function is not as effective

TABLE I. Polarization rate for AGS.

		Pol$_f$/Pol_i	
$nP \pm \nu_z$	ε_0	Gaussian	Simulation
8.7	0.0061	-0.878	-0.765
27.3	0.0051	-0.796	-0.657
44.7	0.011	-0.981	-0.940

as the rf dipole method in overcoming the intrinsic spin resonance in the polarization beam acceleration.

The quadrupole-mode transfer function can also be a powerful tool to measure the machine impedances that cause bunch shape oscillations. In the future, we plan to explore its application in the collective beam instabilities. Correlation among quadrupole-mode monitors can be used to study the σ matrix for the beam transport. The method of the model independent analysis can then be used to analyze the hidden dynamical variables. The quadrupole-mode transfer function (QTF) may also find applications in plasma physics, solid state physics, and other branches of applied physics in controlling and analyzing the stability of these dynamical systems.

APPENDIX A: RESONANCE STRENGTH OF HALF INTEGER SIDEBANDS

We consider N rf quadrupoles distributed in an accelerator, the Hamiltonian for particle motion is

$$
H(y,y') = \frac{1}{2}y'^2 + \frac{1}{2}K_y(s)y^2 + \sum_{i=1}^{N}\sum_{n=-\infty}^{\infty}\frac{B_1(s_i)\ell_i}{2B\rho}
$$
$$
\times \delta(s-s_i-nC)y^2\cos(\omega_m t + \theta_i), \quad (A1)
$$

where s is the longitudinal coordinate along the accelerator, s_i is the location of the rf quadrupole, $B_1(s_i)\ell_i$ is the integrated rf dipole field strength of the ith quadrupole, C is the circumference of the accelerator, ω_m is the modulation angular frequency, and θ_i is the phase of the ith quadrupole. Transforming to the action-angle coordinates, one obtains [15]

$$
H(J_y,\phi_y) = \nu_y J_y + J_y\sum_{i=1}^{N}\sum_{n=-\infty}^{\infty}\frac{B_1(s_i)\ell_i\beta_y(s_i)}{2\pi B\rho}e^{jn(s-s_i)/R}
$$
$$
\times\cos^2\left(\phi_y+\mu_y(s_i)-\nu_y\frac{s_i}{R}\right)\cos(\omega_m t + \theta_i), \quad (A2)
$$

where J_y, ϕ_y are conjugate action-angle coordinates, R is the average radius of the accelerator, and we have used

$$
\sum_{n=-\infty}^{\infty}\delta(s-s_i-nC) = \frac{1}{C}\sum_{n=-\infty}^{\infty}e^{jn(s-s_i)/R}. \quad (A3)
$$

Expanding the Hamiltonian in revolution harmonics, we find

$$
H(J_y,\phi_y) = \nu_y J_y + \frac{J_y}{2}\sum_{n=-\infty}^{\infty}\{A_{n,+,+}e^{j(2\phi_y+n\theta+\omega_m t)}
$$
$$
+A_{n,-,-}e^{j(-2\phi_y+n\theta-\omega_m t)}
$$
$$
+A_{n,+,-}e^{j(2\phi_y+n\theta-\omega_m t)}
$$
$$
+A_{n,-,+}e^{j(-2\phi_y+n\theta+\omega_m t)}\} + h(J_y,t), \quad (A4)
$$

where $\theta=s/R$ is the orbiting angle around the accelerator, $h(J_y,t)$ depends only on the time t and J_y, and

$$
A_{n,\pm,\pm} = \sum_{n=1}^{N}\frac{\beta_i B_1(s_i)l_i}{8\pi B\rho}e^{-jns_i/R\pm j[2\mu_y(s_i)-2\nu_y s_i/R\pm\theta_i]}
$$
$$
= \oint\frac{\beta(s)B_1(s)}{8\pi B\rho}e^{-jns/R\pm j[2\mu_y(s)-2\nu_y s/R\pm\theta(s)]}ds.
$$
$$
(A5)
$$

Note that $d\phi_y/d\theta = \nu_y$. When the modulation tune $\nu_m = \omega_m/\omega_0$ is near a half integer betatron sideband, e.g., $\nu_m \approx 2\nu_y - n$, the stationary phase term in the Hamiltonian dominates the dynamics, and the Hamiltonian can be approximated by

$$
H(J_y,\phi_y) \approx \nu_y J_y + C_1 J_y\cos(2\phi_y-n\theta-\omega_m t+\chi), \quad (A6)
$$

where we identify the Fourier amplitude as $A_{n,-,+} = C_1 e^{-j\chi}$ and neglect all nonresonance terms.

APPENDIX B: TORI FOR NONLINEAR MATHIEU INSTABILITY

The nonlinear Mathieu Hamiltonian can be normalized as follows:

$$
H = \Delta I - c_1 I\cos 2\psi + \frac{1}{2}I^2, \quad (B1)
$$

where $\Delta = \delta/\alpha_{xx}$, $c_1 = -C_1/\alpha_{xx}$. For $c_1 \geq 0$, invariant tori are shown in Fig. 1, and for $c_1 < 0$, the tori are rotated by $90°$. Without loss of generality, we consider $c_1 > 0$. The stable fixed points of the the Hamiltonian (B1) are given by

$$
I_{\text{sfp}} = \begin{cases} c_1 - \Delta & \text{for} \quad \Delta \leq c_1, \\ 0 & \text{for} \quad \Delta \leq -c_1 \quad \text{and} \quad \Delta \geq c_1, \end{cases} \quad (B2)
$$

with $\psi = 0$ and π. The Hamiltonian value of the fixed point is $H_{\text{sfp}} = -\frac{1}{2}I_{\text{sfp}}^2$.

The unstable fixed points are located at

$$
I_{\text{ufp}} = \begin{cases} -c_1 - \Delta & \text{for} \quad \Delta \leq -c_1, \\ 0 & \text{for} \quad -c_1 \geq \Delta \geq c_1, \end{cases} \quad (B3)
$$

with $\psi = \pi/2$ and $3\pi/2$. These fixed points are shown in Fig. 1. The Hamiltonian value of the separatrix torus is $H_{\text{ufp}} = -\frac{1}{2}I_{\text{ufp}}^2$. The minimum action of the separatrix orbit is $I_{\text{sx, min}} = (\sqrt{-\Delta}-\sqrt{c_1})^2$. Thus the aspect ratio of the separatrix orbit is given by $(\sqrt{-\Delta}-\sqrt{c_1})/(\sqrt{-\Delta}+\sqrt{c_1})$.

APPENDIX C: BOLTZMANN DISTRIBUTION IN BEAM

1. Linear system

A beam in thermal equilibrium obeys the Boltzmann distribution $\rho = \mathcal{N}e^{-H/E_T}$, where H is the Hamiltonian, $\mathcal{N}$ is the normalization factor and E_T is the "thermal energy" of the beam. For a linear Hamiltonian with $H = \nu_y J_y$, the Boltzmann distribution becomes Gaussian with

$$
\rho(J_y,\psi_y) = \frac{1}{2\pi\epsilon_0}e^{-J_y/\epsilon_0}, \quad (C1)
$$

where ϵ_0 is the rms emittance of the beam. Normally, the thermal energy of the beam distribution in a linear system is

$E_T = \Omega \epsilon_0$, where Ω is the tune of the Hamiltonian. When an rf quadrupole field is applied to the system, the Hamiltonian becomes $H(\psi, J_y) = \delta J_y + C_1 J_y \cos 2\psi_y$, and the Boltzmann distribution is

$$\rho(J_y, \psi_y) = \frac{1}{2\pi\epsilon_0} \exp\left[-\frac{\delta J_y + C_1 J_y \cos 2\psi_y}{\sqrt{\delta^2 - C_1^2}\epsilon_0}\right], \quad \text{(C2)}$$

where $\Omega = \sqrt{\delta^2 - C_1^2}$. The rms beamwidths of this distribution in the normalized coordinates are

$$\sigma_y^2 = \beta_y \epsilon_0 \left(\frac{\delta + C_1}{\delta - C_1}\right)^{1/2}, \quad \sigma_{P_y}^2 = \beta_y \epsilon_0 \left(\frac{\delta - C_1}{\delta + C_1}\right)^{1/2}, \quad \text{(C3)}$$

where β_y is the betatron amplitude function at the location of measurement. The QTF b_1 can easily be obtained.

2. Nonlinear system

When a nonlinear detuning term is included in the Hamiltonian, the Hamiltonian becomes $H(\psi, J_y) = \nu_y J_y + \frac{1}{2}\alpha_{yy} J_y^2$. The Boltzmann distribution is

$$\rho(J_y, \psi_y) = \mathcal{N} \exp\left\{-\frac{\nu_y J + \frac{1}{2}\alpha_{yy} J^2}{E_T}\right\}, \quad \text{(C4)}$$

where we assume $\alpha_{yy} > 0$. The normalization constant $\mathcal{N}$ and the thermal energy are determined by the conditions: $\int \rho \, dJ_y d\psi_y = 1$ and $\int J_y \rho \, dJ_y d\psi_y = \epsilon_0$, where ϵ_0 is the rms emittance. From these conditions, we find

$$E_T = \nu_y \epsilon_0 \frac{\text{erfcr}(u)}{2u^2[1 - \text{erfcr}(u)]}, \quad \text{(C5)}$$

$$\mathcal{N} = \frac{1}{2\pi\epsilon_0} \frac{2u^2[1 - \text{erfcr}(u)]}{(\text{erfcr}(u))^2}, \quad \text{(C6)}$$

where the reduced complementary error function is

$$\text{erfcr}(u) \equiv \sqrt{\pi} u e^{u^2} \text{erfc}(u)$$

$$= 1 - \frac{1}{2u^2} + \frac{1 \times 3}{(2u^2)^2} - \frac{1 \times 3 \times 5}{(2u^2)^3} + \cdots, \quad \text{(C7)}$$

with the complementary error function defined as $\text{erfc}(u) = (2/\sqrt{\pi}) \int_u^\infty e^{-y^2} dy$, and the parameter u is given by $u = \nu_y / \sqrt{2E_T \alpha_{yy}}$. Since the parameter u depends on E_T, the thermal energy should be solved self-consistently from Eq. (C5). In general, ν_y is much larger than $\sqrt{2E_T\epsilon_0}$ in accelerator, we find $E_T \approx \nu_y \epsilon_0$ and $\mathcal{N} \approx 1/(2\pi\epsilon_0)$. This is the unperturbed Gaussian distribution shown in Eq. (C1), i.e., the nonlinear detuning does not substantially change the beam distribution.

With an rf quadrupole, the effective Hamiltonian in the *resonance rotating frame* is $H(\psi, J_y) = \delta J_y + J_y C_1 \cos 2\psi_y + \frac{1}{2}\alpha_{yy} J_y^2$. If the rf quadrupole is adiabatically turned on, the particle distribution is a function of the Hamiltonian. In particular, the Boltzmann distribution is

$$\rho(J_y, \psi_y) = \mathcal{N} \exp\left\{-\frac{\delta J_y + C_1 J_y \cos 2\psi_y + \frac{1}{2}\alpha_{yy} J_y^2}{E_T}\right\}. \quad \text{(C8)}$$

The normalization constant $\mathcal{N}$ and the thermal energy E_T are determined by the conditions: $\int \rho \, dJ_y d\psi_y = 1$, and $\sqrt{\langle Y^2 \rangle \langle P_y^2 \rangle - \langle Y P_y \rangle^2} = \epsilon_0$, where ϵ_0 is the rms emittance, $Y = \sqrt{2J_y} \cos \psi_y$, $P_y = -\sqrt{2J_y} \sin \psi_y$, and $\langle \cdots \rangle$ is the ensemble average over the beam distribution. Note that we are working in the parametric space where the beam bunch is slightly perturbed, i.e., the phase space has not entered the bifurcation region of the Mathieu instability. Thus we can use the rms emittance to characterize a beam property.

Using the normalization condition, we find

$$2\pi\mathcal{N}\sqrt{\frac{E_T}{2\alpha_{yy}}} I_0\left(\xi\frac{\partial}{\partial u}\right)\left(\frac{\text{erfcr}(u)}{u}\right) = 1, \quad \text{(C9)}$$

where $u = \delta/\sqrt{2E_T\alpha_{yy}}$, $\xi = C_1/\sqrt{2E_T\alpha_{yy}}$, $\text{erfcr}(u)$ is the reduced complementary error function of Eq. (C7), and $I_0(x)$ is the zeroth order modified Bessel function. Using the rms beam-emittance condition, we obtain

$$2\pi\mathcal{N}\frac{E_T}{2\alpha_{yy}}\sqrt{\left[\left(\frac{\partial}{\partial u} + \frac{\partial}{\partial \xi}\right)I_0\left(\xi\frac{\partial}{\partial u}\right)\frac{\text{erfcr}(u)}{u}\right]\left[\left(\frac{\partial}{\partial u} - \frac{\partial}{\partial \xi}\right)I_0\left(\xi\frac{\partial}{\partial u}\right)\frac{\text{erfcr}(u)}{u}\right]} = \epsilon_0. \quad \text{(C10)}$$

Equations (C9) and (C10) can be used to determine the normalization condition $\mathcal{N}$ and the thermal energy E_T of the Boltzmann distribution. Using the property: $I_0(\xi\partial/\partial u)(1/u) = 1/\sqrt{u^2 - \xi^2}$, one can easily verify that the distribution function (C8) reduces to Eq. (C2) in the small detuning parameter limit with $\alpha_{yy} \to 0$.

The quadrupole-mode transfer function b_1 is

$$b_1 = 2\beta_y(\langle Y^2 \rangle - \langle P_y^2 \rangle)$$

$$= -4\pi\beta_y\mathcal{N}\frac{E_T}{2\alpha_{yy}}\left[\frac{\partial}{\partial \xi}I_0\left(\xi\frac{\partial}{\partial u}\right)\frac{\text{erfcr}(u)}{u}\right], \quad \text{(C11)}$$

where variables u and ξ are defined in the previous paragraphs. Using the asymptotic expansion, we can obtain the coefficient b_1 of the quadrupole beam-transfer function.

[1] See, e.g., S. Y. Lee *et al.*, Phys. Rev. E **49**, 5717 (1994); A. Riabko *et al.*, *ibid.* **54**, 815 (1996); D. Jeon *et al.*, *ibid.* **54**, 4192 (1996); M. Bai *et al.*, *ibid.* **55**, 3493 (1997).

[2] J. D. Fox and P. Corredoura, in *Proceedings of the European Particle Accelerator Conference* (Springer-Verlag, Heidelberg, 1992), p. 1079; D. Li *et al.*, Phys. Rev. E **48**, R1638 (1993); D. D. Caussyn *et al.*, in *Proceedings of Particle Accelerator Conference* (IEEE, Piscataway, NJ, 1993), p. 29; D. Li *et al.*, Nucl. Instrum. Methods Phys. Res. A **364**, 205 (1995).

[3] M. Ellison *et al.*, Phys. Rev. Lett. **70**, 591 (1993); M. Syphers *et al.*, *ibid.* **71**, 719 (1993); H. Huang *et al.*, Phys. Rev. E **48**, 4678 (1993).

[4] Y. Wang, *et al.*, Phys. Rev. E **49**, 1610 (1994).

[5] D. Jeon *et al.*, Phys. Rev. Lett. **80**, 2314 (1998); C. M. Chu *et al.*, Phys. Rev. E **60**, 6051 (1999).

[6] M. H. Wang and S. Y. Lee, J. Appl. Phys. (to be published).

[7] M. Bai *et al.*, Phys. Rev. ST Accel. Beams **3**, 064001 (2000).

[8] M. Bai *et al.*, Phys. Rev. Lett. **80**, 4673 (1998); M. Bai *et al.*, Phys. Rev. E **56**, 6002 (1997).

[9] J. Safranek, Nucl. Instrum. Methods Phys. Res. A **388**, 27 (1997).

[10] J. Irwin *et al.*, Phys. Rev. Lett. **82**, 1684 (1999).

[11] F. Z. Khiari *et al.*, Phys. Rev. D **39**, 45 (1989).

[12] S. Y. Lee, *Spin Dynamics and Snakes in Synchrotrons* (World Scientific, Singapore, 1997).

[13] J. Budnick *et al.*, Nucl. Instrum. Methods Phys. Res. A **368**, 572 (1996).

[14] Y. Wang *et al.*, Phys. Rev. E **49**, 5697 (1994).

[15] See, e.g., S. Y. Lee, *Accelerator Physics* (World Scientific, Singapore, 1999).

[16] R. H. Miller *et al.*, in *Proceedings of the 12th International Conference On High Energy Accelerators* (Fermilab, Batavia, IL, 1983), p. 602.

[17] The rms emittance is defined statistically as the beam distribution, i.e.,
$$\epsilon_0 = \sqrt{(\langle x^2 \rangle - \langle x \rangle^2)(\langle x'^2 \rangle - \langle x' \rangle^2) - \langle ((x - \langle x \rangle)(x' - \langle x' \rangle))^2 \rangle}.$$

[18] S. J. Russell *et al.*, in *Proceedings of the Particle Accelerator Conference* (IEEE, Piscataway, NJ, 1995), p. 2580.

[19] A. Jansson *et al.*, in *Proceedings of the Particle Accelerator Conference* (IEEE, Piscataway, NJ, 2001), p. 528.

[20] M. Ellison *et al.*, Phys. Rev. E **50**, 4051 (1994).